URSI GASS 2020, Rome, Italy, 29 August - 5 September 2020

Spatial filtering experiment with the Murchison Widefield Array

Gregory Hellbourg(1) and Ian Morrison(2)
(1) California Institute of Technology, CA, USA
(2) Curtin University, WA, Australia

Abstract

Spatial Radio Frequency Interference (RFI) filtering offers both RFI rejection and potential signal-of-interest recovery. It is as such an attractive RFI mitigation technique for radio interferometry. This paper describes an experiment of spatial filtering of an amateur radio transmission originating from the International Space Station corrupting the Murchison Widefield Array low-frequency radio telescope.

1 Introduction

Radio Frequency Interference (RFI) is threatening radio astronomy due to the rapid development of commercial wireless applications. RFI mitigation in radio astronomy usually consists of detecting and discarding corrupted telescope data [1]. Radio interferometers, such as the Murchison Widefield Array (MWA), also offer the possibility of processing RFI in the spatial domain. Such filtering methods theoretically enable the recovery of astronomical information in corrupted time and frequency data [2].

This paper describes a spatial filtering experiment conducted with the MWA on a radio amateur transmission from an emitter located on the International Space Station (ISS). Section 2 briefly presents the radio telescope and the data set collected for this experiment. Section 3 provides an overview of spatial filtering and the data model it is based on. Section 4 describes the experiment and draws conclusions on its performance.

2 Instrument and data

2.1 Murchison Widefield Array

The MWA [3] is a low frequency (80 - 300 MHz) radio interferometer located in Western Australia. The array consists of 128 tiles of 16 dual-polarization antennas organized on a regular 4×4 grid. Each tile outputs an analog beamformed voltage stream that is then further amplified, digitized, and channelized in 24 × 1.28 MHz-wide channels by dedicated receivers (each receiver processes 8 tiles). The data are then sent to servers to broadcast the tile data onto a private network connected to a correlator and a voltage data capture engine.

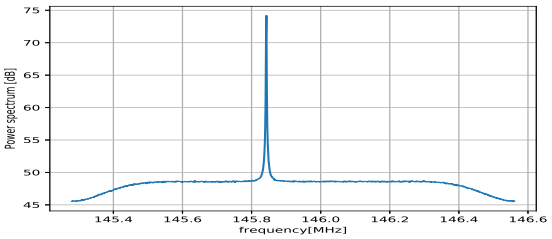

Figure 1. 1.28 MHz-MWA coarse channel power spectrum of data corrupted by a radio amateur transmission. Frequency resolution = 1.25 kHz, integration = 8 seconds.

Despite being located in a remote radio quiet zone, various sources of RFI regularly affect the operation of the MWA [4]. Among the recurring sources of RFI figure communication satellites, such as the ORBCOMM satellite constellation [5, 6], as well as DAB/DVB and FM transmissions reflected from airplanes or meteorites.

2.2 Data set

This paper presents the main results of a spatial filtering experiment conducted on MWA data corrupted by a radio amateur downlink transmission from the ARISS system located on the ISS [7] . The dataset was collected on 2019-07-22 at 15:00:06 UTC, and the full complex voltage stream was recorded for 2 minutes for all 128 dual-polarization tiles, over a 1.28 MHz coarse channel centered at 145.92 MHz. All tiles were beamformed (through analog beamforming) towards the local zenith. A power spectrum at a spectral resolution of 1.25 kHz of the complete observation (after MaxSNR beamforming [8]) is shown in figure 1. The spectrum features a strong peak around 145.84 MHz corresponding to the satellite transmission, and attenuations on the edges of the band due to the coarse channelizing filter bank the data have been pre-processed with.

After further channelization over a 40 kHz frequency bandwidth centered at 145.86 MHz, the details of a digitally modulated signal can be identified on the spectrogram shown in figure 2.(a). Assuming a continuous-power transmission, the satellite appears to approach the center of a MWA main- or side-lobe around 110 s after the start of the observation, as can be interpreted from the mean

power time-variation on the frequency-averaged spectrogram shown in figure 2.(b). A similar conclusion can be made from the brightness time variation of the transmission in figure 2.(a). However, ephemeris of the ISS have not been retrieved to confirm this observation.

The transmission is interrupted every ≈ 5 s to transmit continuous wave (CW) signals. The instantaneous spectrum of the transmission (outside the CW emission windows) follows a sinc pattern, distinctive of Phase-Shift Keying modulation schemes (e.g. [9]). A quadratic frequency-drift spanning ≈ 10.5 kHz over the complete observation can be observed, highlighting the Doppler effect of the accelerated relative motion between the transmitter and the telescope.

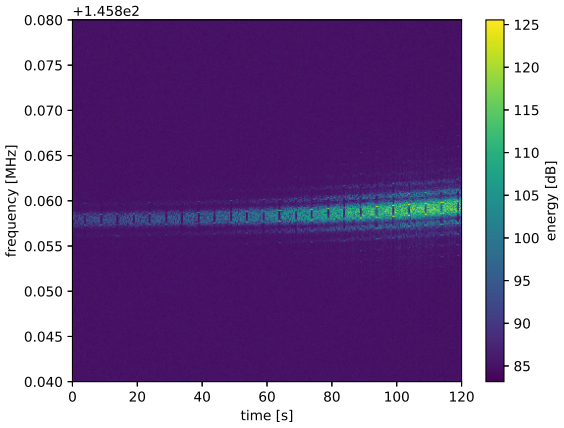

(a)

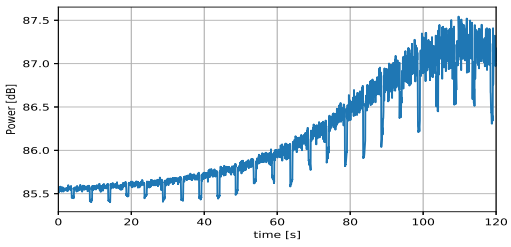

(b)

Figure 2. (a) Spectrogram and (b) Frequency-averaged spectrogram of the radio amateur downlink signal captured during the MWA observation. Frequency resolution = 5 Hz, Time resolution = 205 ms.

3 Spatial filtering

Radio interferometers are less sensitive to RFI than single dish telescopes due to signal de-correlation between antenna-pairs [10]. The attenuation is however insignificant for air- or spaceborne transmitters approaching the steering direction of the synthesized telescope beam, as is the case in this example where the satellite approaches a lobe of the telescope beam .

3.1 Data model

The digitized and channelized voltage data vector collected in this dataset at time sample n, and its correlation matrix at time lag $\tau = 0$, are modeled as follows:

$$\mathbf{x}[n] = \mathbf{a} \cdot r[n] + \eta[n] \tag{1}$$

$$\mathbf{R} = \mathbb{E}\left\{\mathbf{x}[n] \cdot \mathbf{x}^H[n]\right\} = \sigma_r^2 \, \mathbf{a} \cdot \mathbf{a}^H + \mathbf{R}_\eta \tag{2}$$

where $(.)^H$ stands for the conjugate-and-transpose operator, $\mathbf{x}[n]$ is the $(N_a = 128 \times 1)$ array voltage data output vector, $r[n]$ is the RFI baseband signal, $\mathbf{a}$ is the $(N_a \times 1)$ ISS array vector containing complex phase shifts and attenuations for each antenna due to path differences between the emitter and the individual array elements (the transmission is assumed to be narrow band relative to the processed bandwidth). $\eta[n]$ is a $(N_a \times 1)$ system noise vector modeled as a centered white complex Gaussian independent and identically distributed vector with diagonal covariance $\mathbf{R}_\eta$ (i.e. $\eta[n] \sim \mathcal{N}\mathcal{C}(\mathbf{0}, \mathbf{R}_\eta)$). Astronomical sources are here neglected in comparison with the RFI and system noise energy levels.

Correlations between antennas are estimated using short-term sample correlation matrices (SCM):

$$\hat{\mathbf{R}} = \sum_{n}^{N_r} \mathbf{x}[n] \cdot \mathbf{x}^H[n] = \hat{\sigma}_r^2 \hat{\mathbf{a}} \cdot \hat{\mathbf{a}}^H + \hat{\mathbf{R}}_\eta \tag{3}$$

where $\hat{\sigma}_r^2$ is an estimate of the RFI power, $\hat{\mathbf{a}}$ is an estimate of $\mathbf{a}$, and $\hat{\mathbf{R}}_\eta$ is an estimate of $\mathbf{R}_\eta$. We note here that the spatial and temporal stationarity of the model is assumed, i.e. the quantities $\mathbf{a}$ and $\mathbf{R}_\eta$ remain constant over N_r samples. This implies:

- N_r defines a short integration time,
- The relative motion between the emitter and the telescope is negligible, and
- The system noise (including the sky noise) is stationary

High sampling rate data processing is preferred to satisfy both a short data integration time and large N_r to provide consistent covariance estimators.

3.2 Spatial filter

The $(N_a \times N_a)$ orthogonal projection operator [11] is defined as:

$$\mathbf{P} = \mathbf{I} - \mathbf{a}\left(\mathbf{a}^H \cdot \mathbf{a}\right)^{-1} \cdot \mathbf{a}^H \tag{4}$$

with $\mathbf{I}$ standing for the identity matrix.

This operator is applied as a spatial filter either onto the array data vector $\mathbf{x}[n]$ or onto its correlation matrix:

$$\mathbf{x}_p[n] = \mathbf{P} \cdot \mathbf{x}[n] \tag{5}$$

$$\hat{\mathbf{R}}_p = \mathbf{P} \cdot \hat{\mathbf{R}} \cdot \mathbf{P}^H \tag{6}$$

Building the projector $\mathbf{P}$ requires knowledge of the spatial vector $\mathbf{a}$. This vector can only be inferred if perfect calibration of the array is assumed and the location of the RFI emitter is known. None of these conditions are met in the current example. Estimating the quantity $\mathbf{a}$ is therefore necessary, and various approaches have been suggested to

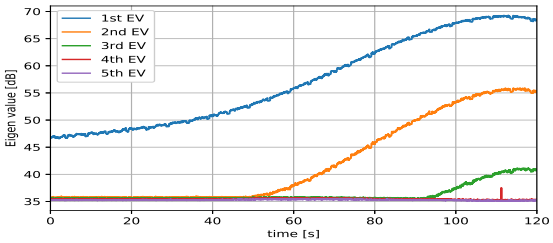

Figure 3. Evolution of the 5 dominant eigenvalues (in dB) of the successive correlation matrices evaluated over N_r =51200 over the duration of the observation.

achieve this [12]. In the context of high Interference-to-Noise Ratio (INR), i.e. $\sigma_r^2 \gg \left\|\mathbf{R}_\eta\right\|_2$ with $\|.\|_2$ the matrix norm 2, an estimate $\hat{\mathbf{a}}$ of $\mathbf{a}$ is the eigenvector corresponding to the dominant eigenvalue of $\hat{\mathbf{R}}$ [11, 12].

4 Data processing

Following the data model given in equation 2, the subspace associated with the RFI is 1-dimensional. The sample covariance matrix is however evaluated over a finite duration, as expressed in equation 3. The RFI subspace of this latter matrix remains 1-dimensional as long as the relative motion between the source of RFI and the telescope is negligible over the integration time ($\propto N_r$). The violation of this hypothesis leads to an increase in dimensionality of the RFI subspace, called *subspace smearing* [13]. Figure 3 illustrates this effect, showing the evolution of the 5 dominant eigenvalues of SCM evaluated over successive (non-overlapping) $N_r = 51200$ samples-long time windows. The dominant eigenvalue remains $\approx$ 10 dB above the other eigenvalues for the first $\approx$ 50 s, validating that the RFI subspace can be expressed as a 1-dimensional subspace. The relative acceleration of the emitter, illustrated by the Doppler-frequency drift in the spectrogram in figure 2.(a), starts increasing after $\approx$ 50 s, similarly to when the second and third larger eigenvalues in figure 3 become dominant compared to the other eigenvalues. The RFI subspace can then no longer be expressed as a 1-dimensional subspace. A short-duration peak can be noticed on the 4th dominant eigenvalue around 110 s. Its origin is unknown, but may be related to a transient RFI or instrument failure.

The projection operator defined in equation 4 can be extended to multi-dimensional subspace projection to account for subspace smearing. The quantity $\mathbf{a}$ can then be replaced with a matrix made of the N_d vectors associated with the N_d dominant eigenvalues of the SCM, where N_d is an estimate of the RFI subspace dimensionality. Model selection techniques [14] such as the Minimum Description Length have been proposed as blind estimators of N_d.

Figure 4 shows the comparison of the impact of multi-dimensional subspace projections on the RFI, with $N_d = 1$ (figure 4.(a)), $N_d = 2$ (figure 4.(b)), and $N_d = 3$ (figure 4.(c)). As expected from the eigenvalue analysis in figure 3, the 1-D subspace projection (figure 4.(a)) is efficient at filtering out the RFI until $\approx$ 50 s. The remainder of the 1-D projected data still contains a significant amount of RFI. The RFI can also be detected at the end of the observation after a 2-D projection (figure 4.(b)). $N_d = 3$ seems to be the appropriate parametrization of the spatial filter, as expected from figure 3.

To compare the RFI attenuation for the 3 evaluated filters, figure 5 shows the averaged spectra over the complete observation duration of the unprocessed data, and the filtered data with $N_d = 1$, 2, and 3. The 1-D projector has a significant impact on the RFI attenuation, with a maximum of $\approx$ 15 dB attenuation. Another 7 dB attenuation is gained by expanding the projector to a 2-D subspace. Finally, the power level of the RFI reaches the system noise floor after 3-D spatial filtering.

Although the attenuation of the RFI signal can be empirically evaluated, nothing can be concluded on the impact of spatial filtering on the system noise subspace, and even on potential non-negligible astronomical sources. The 3-D filter gives the best overall performance in terms of RFI attenuation, but is certainly over-filtering the first 50 s of observation where a 1-D subspace projection was enough to provide an appropriate RFI attenuation. The system noise subspace is affected by this filtering, but this impact cannot be qualified without further astronomical data processing. Moreover, filtering might affect the instrumental calibration. The recovery of the underlying noise subspace has however been addressed and solutions have been proposed in [11, 15].

5 Conclusion

Spatial filtering is an attractive alternative to classic RFI mitigation techniques in radio interferometry as it offers good RFI rejection performance as well as the potential recovery of underlying astronomical sources and system noise.

Subspace smearing due to fast moving RFI is the main performance limitation of the technique as it increases the filtered spatial bandwidth spanned by the RFI, and can therefore affect both the astronomical information recovery and the array noise calibration performance. Over-estimating the increase in dimensionality of the RFI subspace due to the smearing effect is an additional source of telescope data corruption.

The RFI mitigation experiment presented in this paper demonstrates the feasibility of RFI spatial rejection with the MWA. Further performance assessments remain to be conducted, particularly regarding the recovery of signals-of-interest after filtering and classic astronomical data processing. This assessment can be conducted through the comparison between uncorrupted, non-filtered, and filtered images.

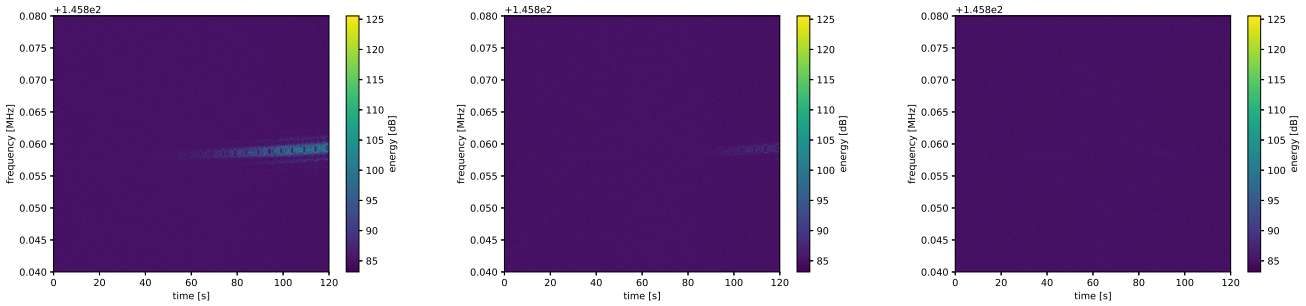

(a) (b) (c)

Figure 4. Comparison of RFI subspace projection after (a) 1D-subspace estimate, (b) 2D-subspace estimate, (c) 3D-subspace estimate.

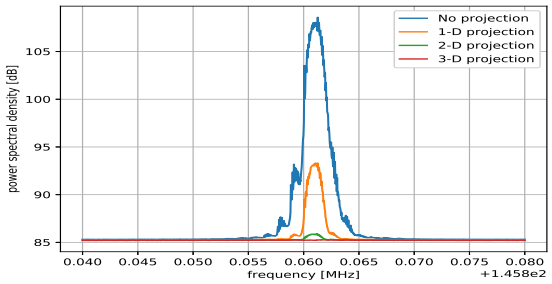

Figure 5. Averaged spectrum after no filtering, 1-D projection, 2-D projection, and 3-D projection.

A GPU version of the spatial filtering algorithm is currently under development, and will be optionally included in the classic data processing pipeline.

References

[1] Offringa, A.R. "Algorithms for radio interference detection and removal." (2012).

[2] Hellbourg, G. Radio Frequency Interference spatial processing for modern radio telescopes. Diss. 2014.

[3] Tingay, S., et al. "The Murchison widefield array: The square kilometre array precursor at low radio frequencies." Publications of the Astronomical Society of Australia 30 (2013).

[4] Sokolowski, M., et al. "The statistics of low frequency radio interference at the Murchison Radio-astronomy Observatory." 2015 IEEE Global Electromagnetic Compatibility Conference (GEMCCON). IEEE, 2015.

[5] Neben, A. R., et al. "Measuring phased array antenna beampatterns with high dynamic range for the Murchison Widefield Array using 137 MHz ORBCOMM satellites." Radio Science 50.7 (2015): 614-629.

[6] Line, J. L. B., et al. "In situ measurement of MWA primary beam variation using ORBCOMM." Publications of the Astronomical Society of Australia 35 (2018).

[7] `https://www.amsat.org/amateur-radio-on-the-iss/`

[8] Van Veen, B. D., and Buckley, K. M. "Beamforming: A versatile approach to spatial filtering." IEEE assp magazine 5.2 (1988): 4-24.

[9] Gardner, W., Brown, W., and Chen, C.-K., "Spectral Correlation of Modulated Signals: Part II - Digital Modulation," in IEEE Transactions on Communications, vol. 35, no. 6, pp. 595-601, June 1987. doi: 10.1109/TCOM.1987.1096816

[10] Perley, R. "Attenuation of radio frequency interference by interferometric fringe rotation." EVLA Memo Series 49 (2002).

[11] Boonstra, A.-J. "Radio frequency interference mitigation in radio astronomy." (2005): 0653-0653.

[12] Hellbourg, G., et al. "RFI subspace estimation techniques for new generation radio telescopes." 2012 Proceedings of the 20th European Signal Processing Conference (EUSIPCO). IEEE, 2012.

[13] Hellbourg, G., "Subspace smearing and interference mitigation with array radio telescopes," 2015 IEEE Signal Processing and Signal Processing Education Workshop (SP/SPE), Salt Lake City, UT, 2015, pp. 278-282. doi: 10.1109/DSP-SPE.2015.7369566

[14] Ding, J., et al. "Model Selection Techniques: An Overview," in IEEE Signal Processing Magazine, vol. 35, no. 6, pp. 16-34, Nov. 2018. doi: 10.1109/MSP.2018.2867638

[15] Leshem, A., and van der Veen, A.-J., "Introduction to interference mitigation techniques in radio astronomy." Perspectives on Radio Astronomy: Technologies for Large Antenna Arrays. 2000.